Chapter 7
Influence of Surface Ultrafine Grain Structure on Cavitation Erosion Damage Resistance

Yaroslav Kyryliv, V. Kyryliv, and Nataliya Sas

7.1 Introduction

Many operational properties of metallic materials, such as fatigue strength, frettage, resistance to wear, corrosion and electrochemical characteristics, and cavitation and erosion damage resistance, depend on the physical and mechanical properties of the surface layer. Destruction of the material begins from the surface. Therefore, the optimization of the surface layer's properties is very important for improving the service life of machine parts and new technologies of metal surfaces processing based on the creation of nanocrystalline (NCS), and ultrafine-grained structures (UFGS) in surface layers are of great interest. In particular, one of the ways to create NCS and UFGS is the grinding of grains in the superficial layer of material to nanometer size. Previous studies have shown that NCS and UFGS can be formed, in particular, by severe plastic deformation (SPD) of the surface. One of these methods is vibration-centrifugal hardening (VCH) [1, 2]. The results of these studies have shown that the VCH forms a high microhardness structure and a significant (up to 7 mm) depth due to the large mass of the strengthening tool. Such structure has better electrochemical characteristics and resistance to wear.

The developed VCH method allows to adjust the mass of the strengthening tool in a wide scope (from 3.5 to 7.5 kg) without increasing the diameter of the balls. Such conditions increase the depth and microhardness of the surface layer by increasing

Y. Kyryliv (✉)
Lviv State University of Life Safety, Lviv, Ukraine

V. Kyryliv
Karpenko Physico-Mechanical Institute of the NAS of Ukraine, Lviv, Ukraine

N. Sas
Stepan Gzhytskyi National University of Veterinary Medicine and Biotechnologies, Lviv, Ukraine

the contact loads in the processing zone [1, 2]. This provides fragmentation and increases the imperfection of the surface layer's structure and allows improving its properties. The main parameters that influence the physical and mechanical properties of the surface layer during the vibration processing are the amplitude and frequency of oscillations, the mass of the tool, the diameter of the balls, and the processing time [1, 2]. In some cases machine parts work under conditions of cavitation erosion damage (CED). The behavior of machine parts after VCH during operation in the CED conditions has not been studied.

The purpose of the work is to study the influence of VCH on cavitation erosion damage resistance and to find optimal VCH modes for increasing cavitation erosion damage resistance of the 40Kh steel.

7.2   Materials and Methods

Rings made from 40Kh steel were used as the samples for research. External and internal diameters of the samples were 75 and 60 mm, respectively, and the width of the samples was 20 mm. Garnished rings of the same steel for the comparative studies of resistance to wear reached the hardness of HRC 52–54. To study the CED, rectangular samples ($140 \times 12 \times 6$ mm; see Fig. 7.1) were made from the rings. Surface *A* of each rectangular sample was strengthened by the VCH. Strengthening was carried out on a special vibration-centrifugal hardening unit [2] with a special massive tool. Balls that were 13 mm in diameter were fixed in the tool. The unit provided vibrations of a certain amplitude and rotation of the tool, as well as its movement along the cylindrical surface. Samples were fixed on a mandrel. The treatment was performed with the following parameters: amplitude of oscillation $A = 5$ mm; frequency of oscillations $f = 24$ Hz; working tool mass $m = 3.5$–7.5 kg; treatment time $\tau = 12$–36 min; and eccentricity $\varepsilon = 10$ mm.

During the VCH treatment, shock dynamic loads act on the surface of a cylindrical sample that carries out vibration oscillations of a certain amplitude and frequency. The loads are made by a special tool of increased mass in the form of a ring with balls fixed in it, which rolls along the outer cylindrical surface of the sample. The material is strengthened as a result of the SPD. The construction of the tool and its mass makes it possible to obtain high contact loads at constant dimensions of the balls. The balls are fixed in the ferrule in the radial direction to the sample. Providing movement of the balls in necessary direction allows increasing the depth of hardening [2].

Microhardness and depth of hardening were measured on the PMT-3 unit according to the standard method (loading on the pyramid was 100 g). The microstructure was investigated on EVO 40XVP scanning electron microscope.

Erosion losses were measured gravimetrically. Before and after tests on cavitation erosion, the samples were washed with acetone and then with ethanol and then dried, and only after that they were weighed on an analytical grade VLA-200 M with an accuracy of ± 0.00005 g.

Fig. 7.1 Schematic illustration of magnetostrictive unit of CED resistance investigation with an undermounted sample
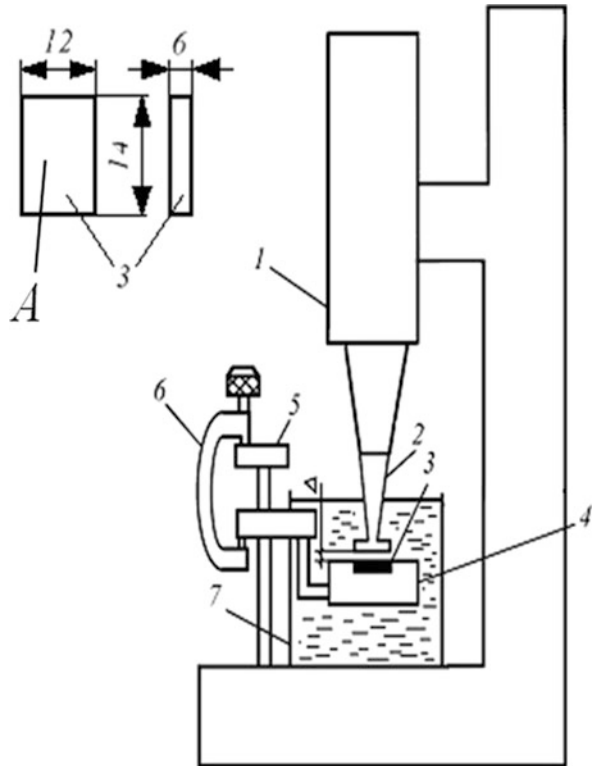
Products of corrosion were usually removed from the surface mechanically, and in some cases samples were steeped into an inhibited pickling solution (5% HCl + 0.15% acid corrosion inhibitor HOSP-10) [3]. After tests, the samples were washed with acetone and ethanol and dried.

The rate of cavitation erosion damage W (g/min•mm^2) was determined by the following formula [4]:

$$W = (m-m_0) / (S \times t),\qquad(7.1)$$

where m and m_0 are the masses of the sample before and after the experiment, g; S is the working area of the sample, mm^2; and τ is the exposure time, min.

The CED resistance was investigated by using the vibration method (using magnetostrictive vibration generator) [4]. According to obtained measurements of cavitation erosion losses, two types of dependencies were constructed. These dependencies characterized the CED of the material and made it possible to evaluate CED resistance of the material. First, for all the studied hydrodynamic modes with oscillation amplitude A (in the case of a magnetostrictive method), the CED kinetic diagrams were constructed in coordinates lg W–lgτ (W, the rate of CED, g/min•mm^2; τ, exposure time, min). They are known to have four main areas [4–6]:

(1) the incubation time τ (involves the time before the registration of mass losses), (2) increasing of W to the maximum value, (3) decreasing of W, and (4) the period of steady destruction, which is characterized by a relatively constant rate of CED (W_{st}). The incubation period of CED in a liquid environment was considered to finish at a time when the CED rate of the material exceeded the rate of corrosion. During the incubation period (as well as under test conditions, when the damage of the cavity surface of the sample was determined by its general corrosion) for calculating W, the working surface of the sample was taken into account. After visual determination of CED, only the part of the surface, on which the traces of damage were detected by the metallographic analysis, was considered for calculating W. According to the kinetic diagrams of the CED, the dependences $\lg W_{st}$–A and $\lg \tau$–A were constructed.

Serial unit UZDN-2 T containing a magnetostrictive generator with a working vibration frequency of 22 kHz was used. The sample, immersed in the liquid, is attached to the tip (Figs. 7.1 and 7.2). The cavitation zone in the unit is created by longitudinal oscillations of the emitter – a nickel rod. These oscillations are excited at the resonant frequency by a magnetostrictive generator. A low pressure area is created under the lower part of the sample which leads to formation of bubbles. During lowering motion, the pressure increases and the bubbles are closed. The amplitude of the oscillations at the UZDN-2 T can be changed within 10–50 μm.

Magnetostrictive tests were carried out with an amplitude of 30 μm in container 7 [4–10] according to the scheme with undermounted sample 3 (Figs. 7.1 and 7.2). Rectangular samples were mounted directly on magnetostrictor emitter 1. Due to the scheme, oscillation concentrator 2 was attached to emitter 1, and sample 3 in the form of a parallelepiped with dimensions of $14 \times 12 \times 6$ mm was fixed in mandrel
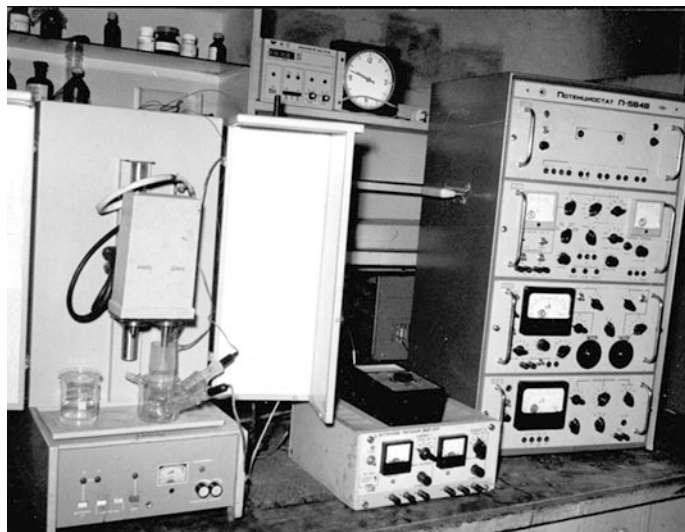

Fig. 7.2 Magnetostrictive unit of CED resistance investigation

4. The mandrel slided on a tripod 5. A micrometer 6 was used to obtain the required physical gap Δ. The value of Δ can significantly affect the CED rate according to such scheme of the tests [4]. During the tests, the gap was fixed at a constant value of $\Delta = 0.5$ mm. According to [4], such value of Δ could lead to obtaining the maximum CED rate. The general view of the test unit is shown in Fig. 7.2.

The tests for cavitation erosion damage (CED) were performed in water with medium hardness (pH 6.3–6.8, hardness 3.8–4.1 mg equivalents/liter). The magnetostrictive tests for undermounted samples were performed according to [11]. Stabilized CED rate W_{st} and incubation period of CED τ_i were chosen as damage parameters.

During the tests, special attention was paid to providing a constant amplitude of oscillations, as there is a direct connection between the amplitude of oscillations and mass loss of the sample.

7.3   Results and Discussion

Preliminary studies, conducted in [1, 2] showed that the optimal parameters for obtaining high microhardness, depth of hardening, favorable corrosion, and electrochemical characteristics are as follows: oscillation amplitude $A = 5$ mm; oscillation frequency $f = 24$ Hz; working tool mass $m = 3.5, 4.5,$ and 7.5 kg; and eccentricity $\varepsilon = 10$ mm. Under these treatment conditions, $t = 28$ min, $\delta = 6$ mm, the microhardness reaches 8.9 GPa (Fig. 7.3), and single-phase structure of the
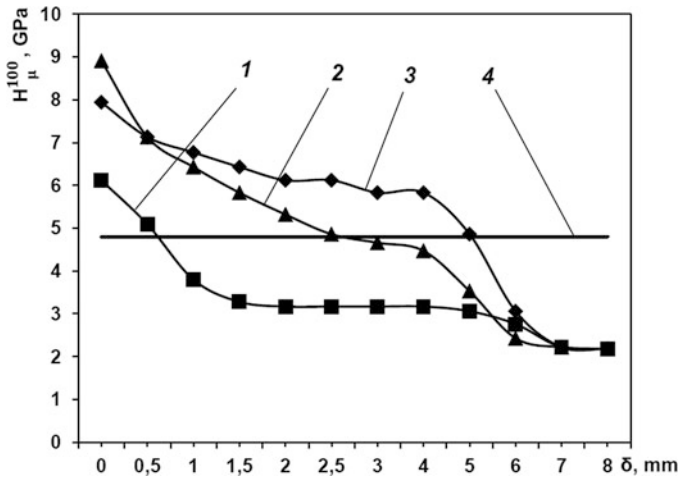

Fig. 7.3 Microhardness of the hardened 40Kh steel layer under various processing methods: (1) VCH ($m_i = 3.5$ kg, $\tau = 20$ min), (2) VCH ($m_i = 4.5$ kg, $\tau = 28$ min), (3) VCH ($m_i = 7.5$ kg, $\tau = 28$ min), and (4) hardening with low tempering (200 °C)
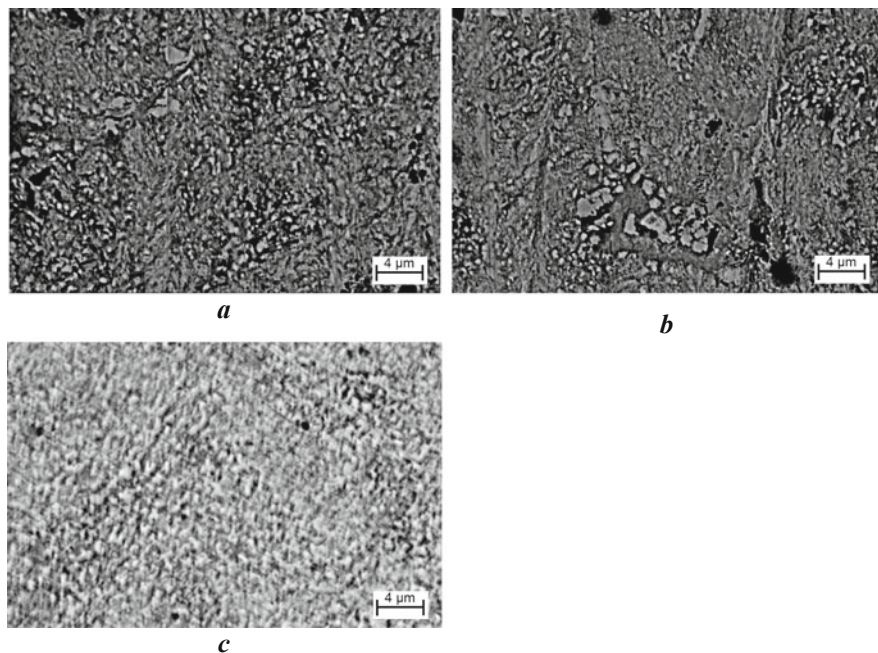
Fig. 7.4 The microstructure of 40Kh steel after VCH at depths: (**a**) 100 μm, (**b**) 1000 μm, and (**c**) matrix structure of 6 mm ($\times$3000) under the following processing modes: $A = 5$ mm; $m = 4.5$ kg; $\tau = 28$ min; and $\varepsilon = 10$ mm

ferritic class (Fig. 7.4) with a grain size on the surface up to 190 nm and a high dislocation density up to 0.84×10^{12} cm^{-2} can be obtained [1, 2, 12].

After the VCH, the microstructure is highly fragmented near the surface at a depth of 100 μm (Fig. 7.4a). The grains are fragmented unevenly by separate blocks. At a depth of 1000 μm (Fig. 7.4b), the picture is similar, and the distribution of grain size decreases, apparently due to a more even distribution of deformation during the impact of the balls' surfaces and smoothly passes to the initial matrix structure (Fig. 7.4c). The steel structure is formed at the optimal processing time $t = 28$ min and the mass of the working tool $m = 4.5$ kg (Fig. 7.4).

One α-phase can be seen in the initial ferritic-pearlitic structure. There are no cementite lines on X-ray patterns, which agrees well with [2] on the decomposition of cementite as a result of cold plastic deformation. In conditions typical for a VCH, such decomposition is possible also at temperatures below the austenite phase existence. The ferrite structure was detected by X-ray studies at all depths within the range of 1 mm. The nature of the lines (110) and (220) [2] indicates large stress in the lattice of the deformed metal. The density of dislocations in the 1 mm section decreases gradually the depth of the metal [2], and this provides a gradient character of the grain size increase. The main increase in microhardness was obtained due to the large voltages in the lattice and the high density of dislocations.

The UFGS has an increased lattice parameter, which decreases in depth. Carbon may segregate at grain boundaries and on dislocation cores or in the form of small graphite precipitates. Dissolution of cementite during the cold deformation leads to redistribution of carbon, which, being placed on the grain boundaries, plays the role of "useful impurities" and blocks the returning processes. High stress in the lattice is the driving force of such redistribution [2].

In order to provide maximum microhardness, the depth of the hardened layer and favorable electrochemical characteristics (Table 7.1) VCH of the samples was performed under the following modes: $m_i = 3.5$ kg, $\tau = 20$ min; $m_i = 4.5$ kg, $\tau = 28$ min; and $m_i = 7.5$ kg, $\tau = 28$ min. By comparison, cavitation erosion tests of steel 40Kh were also performed after samples' processing by traditional technological methods (normalization and machining).

Technological processing methods, including VCH, provide different levels of surface deformation [13]. This has a different influence on the corrosion and electrochemical behavior of 40Kh steel (Table 7.1, Fig. 7.5) as well as cavitation erosion damage resistance. The optimal values of H_μ and the depth of the hardened layer were achieved during VCH under optimal conditions (Fig. 7.3, curves 1–3). VCH provides a significant depth (up to 7 mm) of the hardened layer with a microhardness exceeding the maximum possible value of H_μ (4.8 GPa), which can be achieved by hardening with low tempering (200 °C). The microhardness of 40Kh steel after VCH is higher in comparison with the initial microhardness, and its $H_\mu{}^{max}$ (4.8 GPa) is lower than the microhardness obtained after VCH. Since the CED resistance of materials is determined by the microhardness of the surface, and by corrosion resistance, the above described changes affect the CED resistance of 40Kh steel.

CED resistance of 40Kh steel samples after various technological processing methods differ significantly (Fig. 7.6). The sample after VCH ($m = 7.5$ kg, $\tau = 28$ min) is the most stable in terms of the incubation time τ_i (Fig. 7.6, curve 5). Since the incubation time largely depends on the corrosion resistance of the material, the effectiveness of the technological processing methods' influence on this parameter can be evaluated by the corrosion and electrochemical characteristics of 40Kh steel after processing (Table 7.1, Fig. 7.5).

The positive effect of VCH ($m = 7.5$ kg, $\tau = 28$ min), which is associated with higher corrosion and electrochemical parameters of 40Kh steel after this processing (Table 7.1, Fig. 7.5, curve 5), as well as high level of microhardness and depth of hardened layer, provides surface stability at the stage of damage accumulation. Normalization (Fig. 7.6b, curve 1) also provides some increase of τ_i, but it is lower in comparison to hardening with low tempering because relaxation and redistribution of considerable residual tensile stresses affect the corrosion properties. These residual tensile stresses are usually formed during machining of the samples. VCH under the modes $m = 3.5$ kg, $\tau = 20$ min, and m = 4.5 kg, $\tau = 28$ min, not only does not increase the incubation time but also reduces it in comparison with 40Kh steel in the initial state. After the VCH under these modes, a hardened layer with low level of electrochemical characteristics (Table 7.1 and Fig. 7.5, curves 3 and 4) close to the state of the surface overhardening is

Table 7.1 Mechanical and electrochemical characteristics of 40Kh steel after VCH

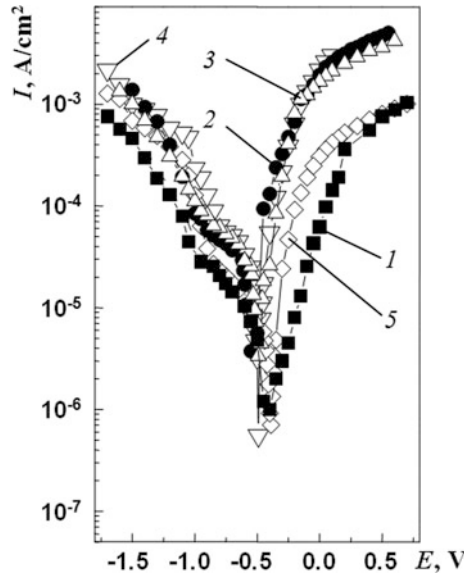| Number	Sample state		Treatment time τ, min	Surface microhardness H_μ^{100}, GPa	Strengthening depth δ, mm	$-E_{cor}$, V	R_p, MΩ/m²	I_a^{max}, A/cm²
	Treatment							
1.	Normalization		–	2.25	–	0.43	64.23	0.0020
2.	Normalization and machining		–	2.8	0.12	0.57	47.13	0.0055
3.	VCH (m_i = 3.5 kg)		6	5.08	4.9	0.45	30.92	0.0020
4.			12	5.83	5.8	0.525	23.14	0.0017
5.			20	6.12	5.8	0.48	26.85	0.0019
6.			28	7.13	5.8	0.46	32.24	0.0025
7.			36[a]	4.12[a]	6.0	0.44	35.87	0.0032
8.	VCH (m_i = 4.5 kg)		6	5.83	5.4	0.47	25.66	0.00057
9.			12	6.43	5.4	0.39	68.06	0.00024
10.			20	7.94	6.7	0.44	72.79	0.00027
11.			28	8.91	6.4	0.49	31.69	0.0030
12.			36[a]	7.94[a]	6.7	0.57	16.83	0.0064
13.	VCH (m_i = 7.5 kg)		6	7.13	6.4	0.53	32.67	0.0028
14.			12	7.13	6.4	0.52	42.74	0.0026
15.			20	7.13	6.4	0.50	45.89	0.0045
16.			28	7.94	6.9	0.39	95.78	0.00036
17.			36	7.94	7.1	0.40	104.28	0.00014

[a]Overhardening

Fig. 7.5 Polarization curves of 40Kh steel after various processing methods: (1) normalization, (2) turning, (3) VCH ($m_i = 3.5$ kg, $\tau = 20$ min), (4) VCH ($m_i = 4.5$ kg, $\tau = 28$ min), and (5) VCH ($m_i = 7.5$ kg, $\tau = 28$ min)
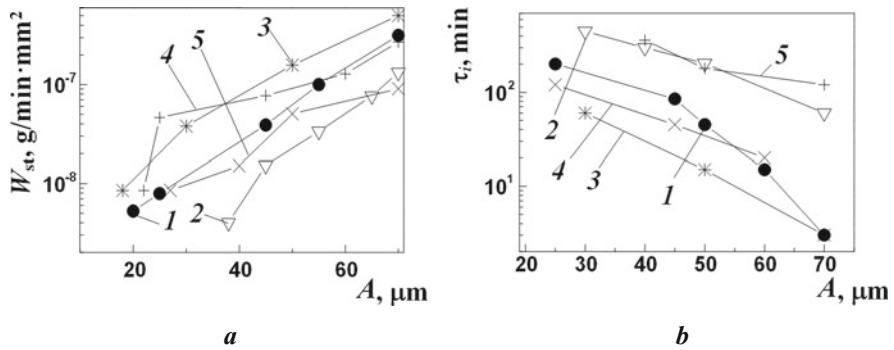

a

b

Fig. 7.6 Dependence of the stabilized CED rate (**a**) and the incubation time (**b**) on the amplitude of testing 40Kh steel samples after technological processing methods: (1, 1) normalization, (2, 2) hardening with low tempering (200 °C), (3, 3) VCH ($m = 3.5$ kg, $\tau = 20$ min), (4, 4) VCH ($m = 4.5$ kg, $\tau = 28$ min), and (5, 5) VCH ($m = 7.5$ kg, $\tau = 28$ min)

formed. According to [14], the corrosion and electrochemical behavior of steels is associated with the degree of their surface deformation, and in particular, in case of overhardening, dislocations reach the metal surface and become dissolution centers [14].

According to the criterion of the stabilized CED rate W_{st} (Fig. 7.6a), the most effective VCH mode is as follows: $m = 7.5$ kg, $\tau = 28$ min. VCH under the modes

$m = 3.5$ kg, $\tau = 20$ min, and $m = 4.5$ kg, $\tau = 28$ min, is not effective according to the criterion τ_i (Fig. 7.6b, curves 3 and 4). These modes provide maximum microhardness due to the achievement of a high defectiveness of the surface layer, close to the overhardening. Since it is believed that the CED occurs according to microfatigue mechanism [15, 16], the presence of a heterogeneous corrosive-active surface with significant defects greatly facilitates the damage of the material. This is due to the relatively insignificant depth and microhardness of the hardened layer in comparison with the depth of CED process (Fig. 7.6, curves 1 and 3).

So, the VCH technology improves the wearing quality of machine parts operating under CED conditions. However, the modes, which bring the material closer to the overhardening according to the degree of the structure imperfection ($m = 3.5$ kg, $\tau = 20$ min, and $m = 4.5$ kg, $\tau = 28$ min), are unsuitable. Modes characterized by lower microhardness, but higher corrosion resistance, are more effective. Such vibration-centrifugal hardening modes, as can be seen from Fig. 7.6, increase the cavitation erosion damage resistance by two times after stabilizing the destruction rate and by ten times at the incubation time.

7.4 Conclusions

Vibration-centrifugal hardening forms on the 40Kh steel surface, an ultrafine-grained ferritic structure with a grain size of 190 nm, dislocation density of 0.84×10^{12} cm^{-2}, and microhardness of 8.9 GPa.

Under certain processing modes, VCH increases the cavitation erosion damage resistance of the surface layer of the strengthened material, mainly due to the increase of the microhardness of the material and the improvement of its corrosion and electrochemical properties. Since the cavitation erosion damage resistance of the material is directly related to the degree of its surface deformation, overhardening of the material leads to decreasing of its CED resistance. For machine parts made of 40Kh steel, working under friction conditions, the best CED resistance is obtained under the following modes of processing: $m = 4.5$–7.5 kg; $\tau = 20$–28 min.

It is shown that vibration-centrifugal hardening increases the cavitation erosion damage resistance by two times after stabilizing the destruction rate and by ten times at the incubation time.

References

1. Aftanaziv IS, Bassarab AI, Kyryliv YB (2002) Mechanical and corrosion characteristics of 40Kh steel after vibration-centrifugal hardening treatment. Mater Sci 38(3):436–441
2. Kyryliv V, Kyryliv Y, Sas N (2018) Formation of surface ultrafine grain structure and their physical and mechanical characteristics using vibration-centrifugal hardening. Adv Mater Sci Eng 2018:3152170

3. Bassarab AI, Zhovnirchuk VM, Tsyrul'nyk OT (2001) Effect of the acid-inhibitor treatment on the resistance of 30Kh GSNA steel to the cavitation-erosion fracture in water. Mater Sci 37(5):820–822
4. Srinivasan Y., Vedula K. (1989) Mechanisms of combined erosion-corrosion of steels at elevated temperatures. A. Levy Ed. Minerals, Metals and Materials Society, Warrendale
5. Pirsol I (1972) Cavitation. Mills And Boon Ltd, London
6. Plesset FJ, Devine RE (1966) Effect of exposure time on cavitation damage. J Basic Eng 68(4):691–705
7. Singh R, Tiwari SK, Mishra SK (2012) Cavitation erosion in hydraulic turbine components and mitigation by coatings: current status and future needs. J Mater Eng Perform 21:1539–1551
8. Knapp R.T., Daily J.W., Hammitt F.G. (1970) Cavitation. McGraw-Hill New York
9. Yabuki A, Noishiki K, Komori K, Matsumura M (2001) The surface behavior of metallic materials during the incubation period of cavitation erosion. ASTMSTP 1339:357–369
10. Karasyuk YA, Kocherov VI, Benino VV, Galaktionova NL (1977) Relationship between corrosion and erosion factors in the cavitation failure of metals. Mater Sci 12(5):537–540
11. Hurei IV, Kyryliv VI, Bassarab AI (2004) Erosion resistance of 40kh steel after mechanical-pulse treatment. Mater Sci 40(2):296–301
12. Nykyforchyn H, Kyryliv V, Maksymiv O (2017) Wear resistance of steels with surface nanocrystalline structure generated by mechanical-pulse treatment. Nanoscale Res Lett 12:150
13. Kyryliv V, Chaikovs'kyi B, Maksymiv O et al (2016) Contact fatigue of 20KHN3A steel with surface nanostructure. Mater Sci 51:833–838
14. Gutman E. M. (1998) Mechanochemistry of materials. Cambridge International Science
15. Ricman RH, McNaughton WP (1990) Correlation of cavitation erosion behavior with mechanical properties of metals. Wear 140:63–82
16. Nykyforchyn HM, Kyryliv VI, Bassarab AI, Voloshyn VA (2002) Wear resistance of mechanical-pulse treated 40kh steel during abrasive friction and cavitation. Mater Sci 38(6):873–879